Time-frequency analysis of scalp EEG with Hilbert-Huang transform and deep learning

Time-frequency Analysis of Scalp EEG with Hilbert-Huang Transform and Deep Learning

Jingyi Zheng, Mingli Liang, Sujata Sinha, Linqiang Ge, Wei Yu, Arne Ekstrom, and Fushing Hsieh

***Abstract*— Electroencephalography (EEG) is a brain imaging approach that has been widely used in neuroscience and clinical settings. The conventional EEG analyses usually require pre-defined frequency bands when characterizing neural oscillations and extracting features for classifying EEG signals. However, neural responses are naturally heterogeneous by showing variations in frequency bands of brainwaves and peak frequencies of oscillatory modes across individuals. Fail to account for such variations might result in information loss and classifiers with low accuracy but high variation across individuals. To address these issues, we present a systematic time-frequency analysis approach for analyzing scalp EEG signals. In particular, we propose a data-driven method to compute the subject-specific frequency bands for brain oscillations via Hilbert-Huang Transform, lifting the restriction of using fixed frequency bands for all subjects. Then, we propose two novel metrics to quantify the power and frequency aspects of brainwaves represented by sub-signals decomposed from the EEG signals. The effectiveness of the proposed metrics are tested on two scalp EEG datasets and compared with four commonly used features sets extracted from wavelet and Hilbert-Huang Transform. The validation results show that the proposed metrics are more discriminatory than other features leading to accuracies in the range of 94.93% to 99.84%. Besides classification, the proposed metrics show great potential in quantification of neural oscillations and serving as biomarkers in the neuroscience research.**

***Index Terms*— Electroencephalography (EEG), Empirical Mode Decomposition (EMD), Hilbert-Huang Transform (HHT), Subject-specific frequency bands, Deep learing (DL)**

I. Introduction

ELECTROENCEPHALOGRAPHY (EEG) is a popular brain imaging technique in various neuroscience research settings [1]. It measures voltage changes through arrays of electrodes placed on the scalps, which reflects the underlying neural activities after attenuation through skin and bones. Distinctive patterns of neural signals are robustly linked to perception, emotion, and other aspects of cognition [1]–[5]. By classifying EEG signal, we can successfully detect the presence of epilepsy [6], microsleep episodes [7], and emotion [8], among others. One prominent phenomenon in EEG signal is the presence of neural oscillations. There are five brain oscillations that are widely recognized: gamma, beta, alpha, theta, and delta. And each brain oscillation corresponds to a well-known frequency band: delta (1-4 Hz), theta (4-8 Hz), alpha (8-12 Hz), beta (12-30 Hz), low gamma (30-60 Hz), etc. [3], [4].

Neural responses are naturally heterogeneous by showing variations between individuals or within individuals. But researchers have been using the same conventional frequency bands to characterize brain oscillations for all individuals. While employing such strict definitions has been useful for advancing our understanding of how specific frequency bands contribute to certain aspects of cognition, the rigidity actually ignores the intrinsic characteristic of brain as a complex system: neural oscillations manifest constant evolving amplitudes and frequencies.

The frequency bands corresponding to brain oscillations might vary across individuals and species. For example, similar behaviors are correlated with oscillations of different frequency bands across animal species: in human hippocampus, movement-related theta oscillations occupy the range of 1-4 Hz, while in rats the frequency range turns to be 4-7 Hz [9]–[13]. Likewise, Doppelmayr *et al.* [14] also argued for individual differences in frequency bands (personalized frequencies) for the measures of event-related band power. Therefore, a rigid categorization of canonical frequency bands might miss the critical aspect of individual differences and instantaneous fluctuation within the oscillatory modes. A method to derive the subject-specific frequency bands is needed.

When quantifying the power of certain brain oscillations, it is common to use the power of several frequencies sampled within the fixed frequency bands, such as the power spectral density (PSD). However, not only the frequency bands of brain oscillations differ across individuals, but also the peak frequencies of oscillatory modes can be different within species. For instance, peak alpha frequencies can shift throughout the development of adulthood [15], and peak alpha frequencies can discriminate the level of sensitivity to pain in individuals [16]. If frequencies sampled within the frequency bands deviate from the intrinsic frequencies related to the

J. Zheng is with the Department of Mathematics and Statistics, Auburn University, Auburn, AL, 36849, USA. e-mail: jingyi.zheng@auburn.edu.

M.Liang and A. Ekstrom are with the Department of Psychology, the University of Arizona, Tucson, AZ, 85721, USA. email: lmliang@email.arizona.edu, adekstrom@email.arizona.edu.

S. Sinha is with the Department of Computer Science and System Engineering, Auburn University, Auburn, AL, 36849, USA. email: szs0210@auburn.edu.

L. Ge is with the TSYS School of Computer Science, Columbus State University, Columbus, GA, USA. email: ge_linqiang@columbusstate.edu.

W. Yu is with the Department of Computer and Information Sciences, Towson University, Towson, MD, USA. email: wyu@towson.edu.

study, information might be lost. Therefore, metrics that can quantify the power of oscillation modes without the need of sampling frequencies is desired.

In addition to pre-processing the scalp EEG signals, the conventional EEG analysis is carried out in several directions: averaging signals on the temporal domain (e.g., event related potentials), transforming signals into frequency domain (e.g., using Fourier Transform) or time-frequency domain (e.g., using Wavelet transform). Features can be extracted accordingly, for example, PSD, entropy, or other statistical features such as standard deviation and mean absolute value of the coefficients or transformed signals [6], [17]–[22]. The features are further used to construct classification models like classifying epileptic EEG signals [6] and differentiating ictal signals [18]. However, the commonly used features are not informative enough to encapsulate individual differences and changes of an oscillatory mode throughout its life span, leading to low accuracy and low robustness of the classification models across individuals. Therefore, it is critical to discover informative features that take individual differences into account while encapsulates meaningful and useful neural information of EEG signals.

To overcome the aforementioned limitations, in this paper, we first propose a data-driven method to obtain the subject-specific frequency bands for brain oscillations. Then, two novel metrics are proposed to characterize the time–frequency representation of sub-signals decomposed from EEG. Three machine learning models are employed to construct classifiers using the proposed metrics on two scalp EEG datasets. Furthermore, classifiers using four commonly used feature sets are also trained to compare the effectiveness of the novel metrics. Additionally, the proposed metrics demonstrate the potential to serve as new biomarkers for neuroscience research.

Our main contributions can be summarized as follows:

- **Data-driven method to obtain subject-specific frequency bands for brain oscillations.** Instead of employing the predefined and fixed frequency bands for all individuals, we propose a HHT-based method to compute the frequency bands for each individual. The results show that the subject-specific frequency bands match the conventional bands closely but they do vary across different subjects.
- **Novel metrics to quantify the power of brain oscillations.** With the subject-specific frequency bands, we propose two novel metrics to measure the frequency and power of the sub-signals obtained from HHT, which can be used to represent brain oscillations. The new information-bearing metrics are more discriminatory than the commonly used feature sets extracted from wavelet transform and HHT in the literatures. Besides, the proposed metrics also carry interpretable meanings in neuroscience.
- **Deep learning-based method to automate feature engineering for HHT.** We propose to automate feature engineering by employing deep learning architectures on the time-frequency representation of EEG signals revealed by HHT.

The remainder of the paper is organized as follows: In Section II, we introduce the two scalp EEG studies. In Section III, we show our proposed approach. In Section IV, we validate the efficacy of our approach on two scalp EEG datasets and compare it with four commonly used feature sets extracted via HHT and wavelet transform. Finally, we conclude the paper and discuss the potential applications of our novel features in Section V.

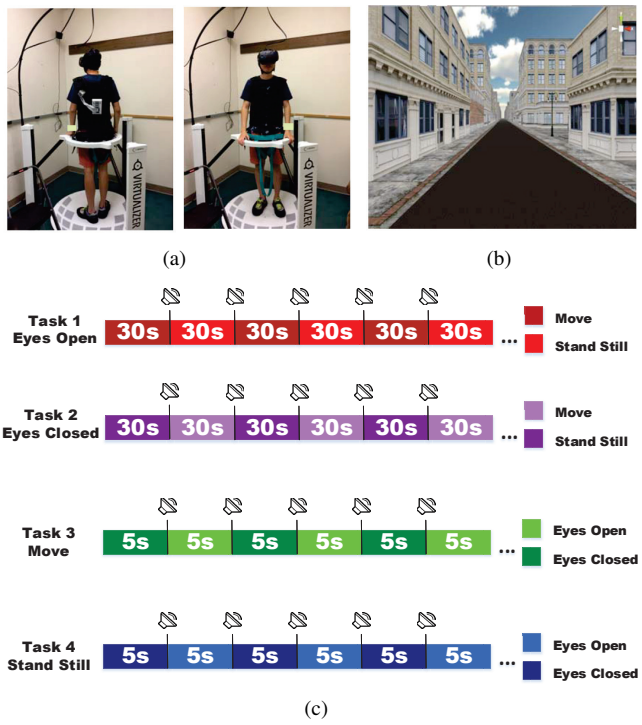

Fig. 1. (a) Front and back of the wireless EEG recording system coupled with an immersive virtual reality and an omnidirectional treadmill. (b) A snapshot of the virtual environment used in the study. (c) Behavioral tasks performed by participants while they underwent scalp EEG recordings. Participants switched between one behavioral state to the other (e.g., in task 1, switching between moving and standing-still), while keeping a constant action (e.g., in task 1, keeping eyes open all along).

II. Scalp EEG Data Description

In this section, we introduce two scalp EEG datasets: study 1 that is used to benchmark our data-driven approach and study 2 that is used to validate the proposed method.

A. Study 1

18 (9 females, 9 males) undergraduate students were invited to participate in this study[1]. EEG was recorded using the BrainVision wireless ActiCap 64-channel scalp EEG recording system (Brain Products GmbH, Germany), with impedances kept below 25 kΩ. Sampling rate was set to 500 Hz, and the reference site was FCz. Signals were then wirelessly transmitted via the MOVE module (Brain Products). A 1-30 Hz bandpass filter was applied to the EEG signals, and anomaly electrodes showing excessive voltages were removed

[1]Written informed consent was obtained before the experiment, and the methods were approved by the ethical review board at University of California, Davis.

and interpolated. Independent component analysis [23] was used to ameliorate eye-blink and muscle artifacts from the EEG dataset. The EEG signals were epoched with the start of epochs aligned to the auditory cues (see Figure 1(c)), and the end of epochs aligned to the start of the subsequent auditory cues. More details of experimental design and data preprocessing can be found in [24].

All participants first underwent placement of scalp EEG recording electrodes and assays of recording quality by the experimenter. When EEG was recorded, participants completed four tasks sequentially. In task 1, they kept their eyes open and switched between walking and standing still for 30 seconds each. In task 2, they kept their eyes closed and switched between walking and standing still for 30 seconds each. In task 3, they alternated between eyes-opened and eyes-closed for 5 seconds each while walking constantly. In task 4, they alternated between eyes-opened and eyes-closed for 5 seconds each while standing still (see Figure 1(c)). For subjects 1-5, each trial in task 3 and 4 last 30 seconds. The number of trials each individual conducted in the four tasks are summarized in Table I.

B. Study 2

We tested 19 adults (7 females, 12 males) from the University of Arizona community[2]. Participants were placed in an immersive virtual reality, and completed a spatial distance monitoring task. In the spatial distance task, participants monitored two possible distances: a short (100 meters) or a long (200 meters) distances. EEG data were recorded and the periods (5.656 seconds long) when participants were monitoring the distances were epoched. Each participant completed 24 repetitions for monitoring each distance, summing up to a total of 48 trials in the spatial distance task.

The continuous EEG was recorded with a 64-channel BrainVision ActiCAP system, which included a wireless transmission MOVE module, and two BrainAmp amplifiers (BrainVision LLC, Morrisville, NC). The reference electrode was FCz. A 1-50 Hz bandpass filtered was applied to the continuous data. Artifact subspace reconstruction (ASR) was then applied for artifact amelioration. Independent component analysis and an automatic component selection procedure, ICLabel [25] were used to correct eye/muscle artifacts. The data is available at https://osf.io/3vxkn/. For more details in experimental design and data preprocessing, please see [26].

C. EEG Notation

For the illustration purpose, we take the EEG recording of one participant conducting task 1 in study 1 as an example. Denote the scalp EEG signal recorded from the j^{th} electrode channel during the k^{th} trial as $x_j^k(t)$. For task 1, the length of the signal is around 30 seconds and the label of $x_j^k(t)$ is binary (i.e., walking or standing still). Our process unit is $x_j^k(t), j = 1, \ldots, 64, k = 1, \ldots, K$ in the following sections. The number of trials K varies among individuals and tasks, which are summarized in Table I. We will implement the following process on each $x_j^k(t)$ for all j and k. To avoid any confusion caused by more subscripts, we will simply use $x(t)$ to denote $x_j^k(t)$ for the purpose of illustration.

[2]Written informed consent was obtained in accordance with the Institutional Review Board at the University of Arizona.

TABLE I
NUMBER OF TRIALS IN TWO SCALP EEG STUDIES

Study 1 (16 Subjects)								
Subject	1	2	3	4	5	6	7	8
Task 1	17	17	18	14	16	8	9	8
Task 2	17	16	16	16	16	9	8	11
Task 3	17	16	16	14	16	44	3	33
Task 4	17	17	15	13	16	38	35	27
Subject	9	10	11	12	13	14	15	16
Task 1	8	16	16	17	16	18	8	16
Task 2	8	12	14	12	16	16	12	16
Task 3	46	69	72	94	47	44	77	64
Task 4	25	36	32	42	24	35	37	31
Study 2 (19 Subjects)								
Each subject conducted 48 trials in the teleportation task								

III. Our Approach

For high dimensional non-linear and non-stationary EEG signals, our goal is to identify the hidden modes of oscillations, and further capture their time-resolved frequency shifts and amplitude spectra in novel feature sets. The process can be carried out in the following steps:

- *Step 1*. Decompose the EEG signal into a set of sub-signals that represent different modes of oscillations and obtain the time-frequency representation of each sub-signal.
- *Step 2*. Compute the subject-specific frequency bands for each brain oscillation.
- *Step 3*. Construct novel feature sets to capture the frequency and power shifts of sub-signals.
- *Step 4*. Draw statistical inference and construct classification models with the proposed feature sets.

By merging the last two steps, we also leverage deep learning architectures to automate the feature engineering process and classify EEG signals.

A. Hilbert-Huang Transform

To explore the hidden modes of oscillations of EEG signals and further monitor their temporal dynamics, we employ the Hilbert-Huang Transform (HHT) [27]. Different from other methods (e.g. wavelet-based transform, fourier transform) that require a set of predefined basis, HHT is a data-driven decomposition method that derives a complete and adaptive basis, from which we can identify the oscillation modes. Specifically, HHT is composed of two major steps, Empirical Mode Decomposition (EMD) and Hilbert spectral analysis.

1) Empirical Mode Decomposition (EMD): EMD is a purely data-driven method that decomposes a signal $x(t)$ into a set of sub-signals with significantly different modes of oscillations. The sub-signal $c_i(t)$ is defined as the Intrinsic Mode Function (IMF) if it satisfies the following two conditions [27]:

- *Condition 1*. The difference between the number of extrema and the number of zero crossings must either be zero or at most one.

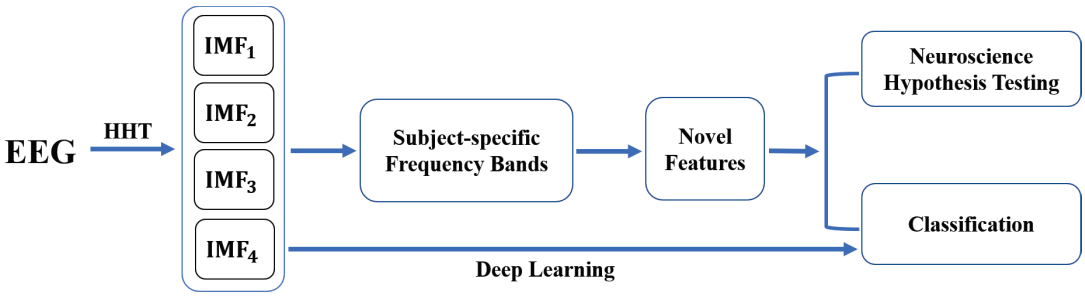

Fig. 2. Block diagram of the propose method.

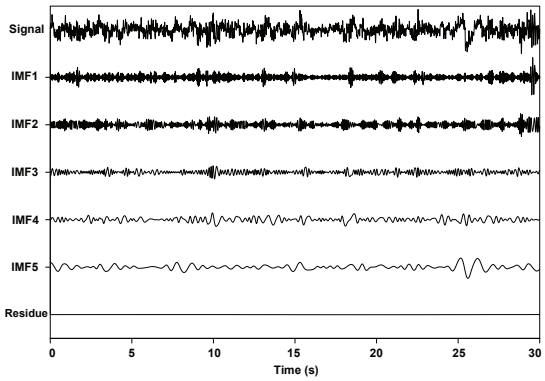

Fig. 3. Outputs of Empirical Mode Decomposition of the EEG signal (top): 8 IMFs and the residue. We show the first five IMFs as the rests are oscillations in lower frequency range.

- *Condition 2.* The mean value of the two envelopes, defined by connecting the local maxima and minima using cubic spline respectively, must be zero at any time point.

The set of IMFs $\{c_i(t), i = 1, \ldots, n\}$ constitutes a complete, adaptive and nearly orthogonal basis for the original signal. The IMFs can be obtained via an iterative sifting process [27]. With EMD, the decomposition of the EEG signal can be written as the sum of all IMFs and a residue that is a trend or a constant.

$$x(t) = \sum_{i=1}^{n} c_i(t) + r_n(t). \tag{1}$$

Figure 3 illustrates the decomposed IMFs using an EEG signal $x_j^k(t)$. The sifting process automatically achieves the trend removal, and the obtained IMFs have zero reference levels, which is a necessary condition to ensure the instantaneous frequency computed from Hilbert transform is physically meaningful.

2) Hilbert Spectral Analysis: Hilbert transform (HT) is a linear operator that takes a signal $x(t)$ and produces its harmonic conjugate $y(t)$, that is

$$y(t) = \frac{1}{\pi} P \int_{-\infty}^{\infty} \frac{x(\tau)}{t - \tau} d\tau, \tag{2}$$

where P is the Cauchy principle value. With HT, we can derive the analytic representation of $x(t)$ as Equation (3), where i is the imaginary unit, and further calculate the instantaneous amplitude $a(t)$ as Equation (4) and instantaneous frequency as Equation (5) in order to timely monitor its frequency shifts and amplitude changes.

$$z(t) = x(t) + iy(t) = a(t)e^{i\theta(t)}, \tag{3}$$

$$a(t) = (x(t)^2 + y(t)^2)^{1/2}, \tag{4}$$

$$\theta(t) = tan^{-1}\frac{y(t)}{x(t)}, \omega(t) = \frac{d\theta(t)}{dt}, \tag{5}$$

Therefore, the original signal $x(t)$ can be represented in a time-frequency-amplitude (or energy, the square of amplitude) representation. However, HT requires the signal to have a zero reference level [27]. For signals riding on a nonzero reference, the instantaneous frequency might have negative values that cannot be interpreted.

HHT breaks the limitation of HT by applying HT on the sub-signals $c_i(t)$ instead of the original signal $x(t)$ because $c_i(t)$s have zero reference levels. With HT, we can obtain the instantaneous frequency $\omega_i(t)$ and instantaneous amplitude $a_i(t)$ for each $c_i(t)$. Therefore, the original signal $x(t)$ can be expressed as

$$x(t) = \sum_{i=1}^{n} Re\{a_i(t)exp(i\int \omega_i(t)dt)\}, \tag{6}$$

where Re denotes the real part of a complex number and the residue $r_n(t)$ is left out. Importantly, the frequency and amplitude obtained from HHT are both functions of time, which are different from Fourier transform with constant frequency and amplitude as in Equation (7).

$$x(t) = Re\{\sum_{i=1}^{\infty} a_i e^{i\omega_i t}\}. \tag{7}$$

To some extent, HHT represents a generalized Fourier transform, lifting the restriction of constant frequency and amplitude. With variable frequency and amplitude, HHT is capable of explaining the non-stationarity of the signal more efficiently. Figure 4 visualizes the time-frequency-amplitude representation (also known as Hilbert-Huang spectrum or Hilbert spectrum) of the IMF_1 (i.e. $c_1(t)$), with the instantaneous frequency $\omega_1(t)$ against time t, colored by the instantaneous amplitude $a_1(t)$.

B. Subject-specific frequency bands for brain oscillations

As discussed before, there are individual differences in frequency bands [14] for brain oscillations. Instead of using

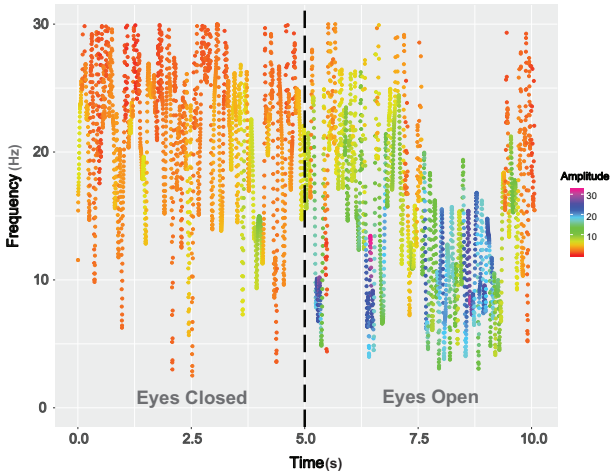

Fig. 4. Hilbert Spectrum of IMF1 from an example EEG signal. In the 10-second signal, the human participant keeps eyes closed during 1-5 seconds, and keeps eyes open during 5-10 seconds. The color represents the instantaneous amplitude (IA), Y-axis represents the estimates of the instantaneous frequencies, and X-axis is the time.

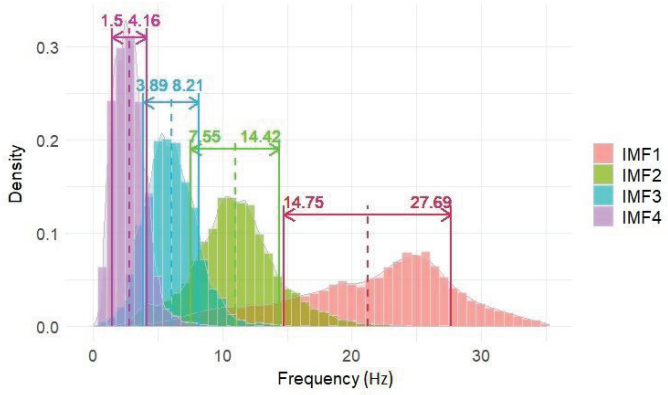

Fig. 5. Empirical distribution of the instantaneous frequency (IF) of IMF 1-4. The EEG signal is from channel 2 during the first epoch while the participant is conducting task 1 (i.e., $\boldsymbol{x_2^1(t)}$). For each IMF, the sample mean is indicated by the dashed line and the interval of $\pm$ one standard deviation from the mean is marked by the solid lines.

a predefined and fixed frequency bands for all subjects, we propose to compute the personalized frequency bands for each individual.

Given $x(t)$, we first decompose it into a set of IMFs, which are in descending order of frequency. The instantaneous frequencies of the last several IMFs are mostly below 0.5 Hz. In both scalp EEG datasets, the apriori research hypotheses focus on 1-30 Hz neural oscillations [24], [26]. Therefore, in the current study, we select the first four IMFs that show frequencies above 1 Hz. It is worth noting that the number of IMFs to keep (i.e., N) depends on the research questions and brain oscillations of interest.

For each of the first four IMFs, we first exam the distribution of their Instantaneous Frequencies (IFs), as shown in Figure 5 with sample means indicated by dashed lines and intervals (i.e., sample mean $\pm$ one standard deviation) marked by solid lines. Each IMF represents distinct modes of oscillations with varying frequency lying in different bands. The reason for

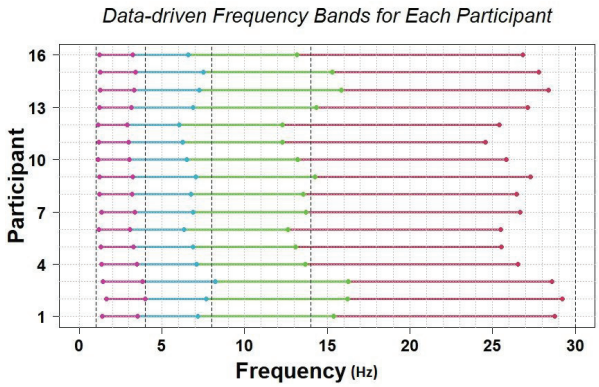

Fig. 6. Data-driven frequency segmentation for 16 participants. Dashed lines indicates the four canonical frequency bands. The colors indicate from which IMF the initial intervals are computed, namely, IMF1 (red), IMF2 (green), IMF3 (blue), and IMF4 (purple).

choosing the intervals with one standard deviation is due to the fact that the frequency bands for different brain oscillations are non-overlapping. Then, we compute the four $\bar{X} \pm 1s$ intervals for signals recorded on the same individual, i.e., signals from all channels, all trials and tasks. After averaging the intervals for each IMF, we obtain the initial frequency bands. To make them non-overlapping, we average the upper/lower boundaries of the consecutive intervals and use it as the frequency bands cut-off. For the example subject, our final segmentation is $R_1 = [14.1, 27.5], R_2 = [7.7, 14.1), R_3 = [3.8, 7.7), R_4 = [1.1, 3.8)$. Figure 6 also summarizes the subject-specific frequency bands for all participants in study 1, with the canonical frequency bands (i.e., delta (1-4 Hz), theta (4-8 Hz), alpha (8-14 Hz), and beta (14-30 Hz)) [**?**], [3], [4] marked in dashed lines. It is clear that the subject-specific frequency bands vary by individuals due to the differences in their neural responses, but they also match the canonical frequency bands closely.

C. Feature Engineering: Creating Novel Feature Sets

As revealed by the Hilbert spectrum in Figure 4, the overall frequencies shift down to a lower frequency range and the overall amplitudes increase when the participant switched from eyes closed to open. The goal of feature engineering is to capture the subtle differences in the Hilbert spectrum of IMFs so as to accurately classify EEG signals.

Moreover, when measuring the power of certain brain wave, the common way is to sample several frequencies in its corresponding frequency bands, then compute the PSD of the sampled frequencies, and use all of them to quantify the power of the brain wave. However, information loss might occur if the sampled frequencies deviate from the intrinsic frequencies of the oscillatory modes. Therefore, the metrics are also designed to identify the IMF that can be representative for certain brain oscillation and offer a simple measure to quantify the power of the brain wave.

1) Frequency Ratio (FR): Denoting the subject-specific frequency bands as $R_s, s = 1, \ldots, S$. Given one IMF $c_i(t), i = 1, \ldots, N$, we record the total amount of time when its IFs $\omega_i(t)$ lie within each frequency bands R_s. To make it compa-

rable between signals with different length, we scale it by the length of the signal T as following.

$$fr_{i,s} = \{(\frac{|\{t|\omega_i(t) \in R_s\}|}{T}), i = 1, \ldots, N, s = 1, \ldots, S\}. \tag{8}$$

In our case, $S = 4$ because we are interested in four brainwaves (i.e., delta, theta, alpha, and beta oscillations), and $N = 4$ because the rest of IMFs are oscillations below 0.5 Hz. The vector $FR_i = (fr_{i,1}, \ldots, fr_{i,4})$ represents the portfolio of the four oscillation modes for the i^{th} IMF. With FR_i, the shifts of the portfolio for the sub-signal can be captured. Moreover, FR_i is also be used to identify the IMF that can serve as a representative for certain brain oscillation. Depending on the largest $fr_{i,s}$ in FR_i, the i^{th} IMF can be representative for the brain oscillation whose frequency band is close to R_s. For instance, $FR_1 = (76.1\%, 12.3\%, 3.0\%, 0.1\%)$ implies that the 1^{st} IMF can be representative for beta oscillation.

2) Averaged Amplitude (AA): If we write the instantaneous amplitude as a function of frequency and time $H(\omega, t)$, the marginal Hilbert spectrum $h(\omega)$ is defined as

$$h(\omega) = \int_0^T H(\omega, t)dt,$$

where T is the length of the signal [27]. $h(\omega)$ provides an alternative spectrum expression to the Fourier spectrum, representing the accumulated amplitude (or energy) over the entire time and measuring the total amplitude contributed by each frequency. Nonetheless, the marginal spectrum is not comparable for signals with varying length, and is for a specific frequency instead of a frequency band. Therefore, we propose the following metric for the i^{th} IMF:

$$\begin{aligned} aa_{i,s} = \{&m(\{H(\omega_i, t)|\omega_i(t) \in R_s\}), \\ &i = 1, \ldots, N, s = 1, \ldots, S\} \end{aligned} \tag{9}$$

where $m(\cdot)$ denote the arithmetic mean. The vector $AA_i = (aa_{i,1}, \ldots, aa_{i,4})$ represents the averaged amplitude over the time period when the IFs fall in each of the four frequency band $R_s, s = 1, \ldots, 4$. AA_i serves as a simple but effective metric for measuring the power of different modes of oscillations. In addition, $aa_{i,s}$ can be used to quantify the power of brain oscillations. For instance, if IMF1 is used to represent the beta wave as indicated by FR_1, then $aa_{1,1}$ measures the power of the beta wave.

Compared with the conventional approach that requires sampling frequencies and computing the power (or the marginal spectrum) of each sampled frequency respectively, the proposed metrics (FR and AA) avoid the problem of sampling frequencies and quantifying the power of brainwaves using multiple measures. Moreover, the metrics can greatly reduce the dimension of the Hilbert spectrum of IMFs.

D. Classification

To test the effectiveness of the proposed metrics in Section III-C, we use them as features to construct classifiers. In study 1, participants are asked to carry out four different tasks. For each task, they switch either body movements or eye movements. In study 2, participants only conduct the spatial teleportation task to identify short vs long distance. Therefore, five binary classifiers are constructed for each task in study 1 and 2, respectively.

Given the signal $x(t)$, the feature vector (FR_i, AA_i) can be extracted for each IMF. Considering the brainwaves we are interested, the feature vectors of the first four IMF are kept. For signals recorded from each of the 64 channels during one trial, we repeat the process and extract the proposed feature sets, which gives 64x32 number of features in total. Considering the limited number of trials compared to the high dimensional features, we employ random forest (RF) to construct the classifier. As an ensemble learning method, RF applies the bagging technique to construct a multitude of decision trees, which reduces the variance at the cost of a small increase in the bias. Different from bagging, RF selects a random subset of features at each split to reduce the correlation between trees in the bootstrap sample, which also enables RF to handle high-dimensional feature space.

Instead of directly using the 64x32 dimension features in RF, we first rank the features according to the Gini impurity which measures the amount of impurity decrease caused by each feature in average. Then, we keep the top $50 \sim 100$ features in the RF, the exact number of features to be kept is chosen according to the classification accuracy. Other feature selection methods such as Boruta and Recursive Feature Elimination can be employed as well. We then optimize the RF classifiers using grid search and cross validation. For both studies, we use 80% trials to train the model and the rest 20% as testing set. Besides RF, we also employ support vector machine (SVM) and XGboost to construct the classifiers. It turns out that RF shows the highest classification accuracy. Moreover, we also extract the commonly used features in the literatures from HHT and wavelet transform to build RF classifiers and compare their performance with the one using proposed metrics. The detailed results are summarized in the next section.

E. Deep Learning

Recently, researchers start to leverage deep learning models for analyzing EEG signals, and neural network architectures have demonstrated the potential of EEG-based brain mapping and classification tasks. For example, research efforts [28], [29] used convolutional neural network (CNN) to classify EEG motory signals; Tabar *et al.* [30] demonstrated the design and training of CNN and stacked autoencoders to decode task related information from raw EEG without handcrafted feature selection. In the BCI competition II, a deep learning classifier [31] with wavelet transformed time-frequency images as input achieved 90% accuracy. Dose *et al.* [32] observed an accuracy of 80% using a convolutional network based architecture with training conducted on over 100 subjects. Likewise, Vrbancic *et al.* [33] used convolutional neural networks on 13 subjects and observed an accuracy of 69%. Therefore, besides using conventional machine learning models with engineered features, we leverage convolutional neural network to construct the classifiers.

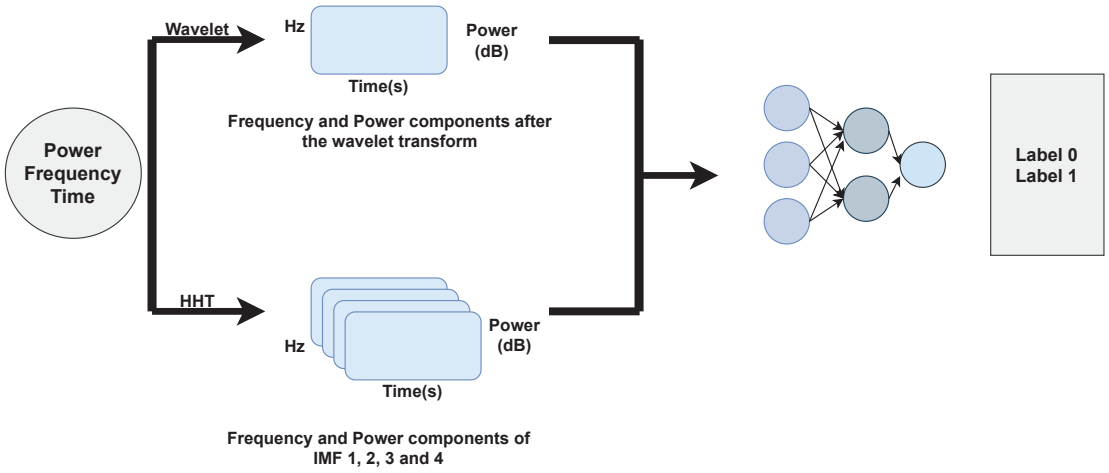

Fig. 7. Deep Learning Framework demonstrating Wavelet and HHT transformed signals served as input to the neural network architecture

TABLE II
CONVOLUTIONAL NEURAL NETWORK ARCHITECTURE WITH SPECIFICATION FOR EACH LAYER

Layer (type)	Specifications
2D Convolutional	filters = 64 X 64 kernel size = (3, 3) activation function = relu
Max Pooling 2D	pool size = 2 X 2
2D Convolutional	filters = 64 X 64 kernel size = (3, 3) activation function = relu
Max Pooling 2D	pool size = 2 X 2
2D Convolutional	filters = 128 X 128 kernel size = (3, 3) activation function = relu
Max Pooling 2D	pool size = 2 X 2
Flatten	-
Dropout Layer	drop out level = 50%
Dense Layer	output space dimensionality = 1 activation function = sigmoid

TABLE III
SEQUENTIAL NEURAL NETWORK MODEL WITH DENSE LAYERS AND SPECIFICATION FOR EACH LAYER

Layer (type)	Specifications
Flatten	-
Dense Layer	output space dimensionality = 128 activation function = relu
Dropout Layer	drop out level = 50%
Dense Layer	output space dimensionality = 128 activation function = relu
Dropout Layer	drop out level = 50%
Dense Layer	output space dimensionality = 1 activation function = sigmoid

TABLE IV
SEQUENTIAL NEURAL NETWORK MODEL (FOR STUDY 2) WITH SPECIFICATION FOR EACH LAYER

Layer (type)	Specifications
Flatten	-
Dense Layer	output space dimensionality = 64 activation function = tanh
Dense Layer	output space dimensionality = 64 activation function = tanh
Dense Layer	output space dimensionality = 1 activation function = sigmoid

In 2018, Acharya *et al.* [34] achieved an accuracy of 88.67% by training a 13-layer convolutional neural network to classify EEG signals. In our work, the deep learning models draw inspiration from the works of Acharya *et al.* and Vrbancic *et al.* [33]. While convolutional layers, pooling layer, and a fully connected layer were used in their work, we have also experimented with dense layers as the output layer (Table II) or all dense layers (Table III and IV).

Time-frequency representations of EEG signals are obtained via HHT and Morlet Wavelet transformations, respectively. Figure 7 demonstrates the pipeline where these representations are fed into a convolutional neural network to obtain classification outcomes. The input to the deep learning model is a 4D array that carries power, frequency, and time as single-precision float values. A single unit dense layer with label 0 or label 1 serves as the output. For example, label 0 in study 1 task 3 represents eyes-opened and 1 represents eyes-closed.

For each of the four tasks in study 1, two deep learning (DL) architectures with convolutional layers (Table II) and without convolutional layers (Table III) are trained. The neural network architecture with convolutional layers (Table II) has three 2D convolutional layers followed by max pooling layer. The number of filters is increased from 64 $\times$ 64 to 128 $\times$ 128 as we proceed from the fourth layer to fifth layer. A similar architecture was used by Acharya *et al.* with more hidden layers and more neurons for the hidden layers (4029 $\times$ 4, 2046 $\times$ 4 and so on). However, our experiments observe better outcomes with lower neuron values than with over 4000 neurons per layer. Like previous work [33], [34], max pooling layer is also used to offer an abstract representation of the features, thereby reducing overfitting. Besides, we have also added dropout layers to offer generalization.

We test our models on hyperparameters including learning rate, filter size, and stride values employed by various previous

works [28]–[30]. Extensive experiments are conducted by varying the learning rate from 0.0001 to 1.0, the epoch values from 50 to 2000, etc. Various loss functions including binary cross-entropy, categorical cross-entropy, absolute error loss, and hinge loss are tested as well. During the model training, the data is divided as 8:2 train-validation sets. The networks are optimized using Adam [35], a gradient based optimization technique. In the final models, we use parameter values and loss functions that offer the highest accuracy: the optimal patience and epoch values are 200 and 500, respectively, the learning rate is 0.001, and the model with binary cross-entropy as the loss function shows higher accuracy.

Since deep learning models are fueled by big data, unavailability of large enough dataset can result in low classification accuracy. Considering the size of our data in study 1, we also test the model without convolutional and max pooling layers (i.e. Table III), which shows the optimal performance. For study 2, three neural network architectures (Tables II, III and IV) are trained. The DL architecture described in Table IV yields the highest accuracy values. Stratified 6-fold cross validation is then employed for model validation. The model performance is summarized in Table VIII in the following section.

TABLE V
COMPARISON OF DIFFERENT METHODS USING THE PROPOSED METRICS

	SVM	Random forest	XGboost
Task 1	96.61*(5.01)	**99.84**(0.65)	97.19*(4.35)
Task 2	91.57*(11.66)	**99.67**(1.30)	92.38*(11.23)
Task 3	90.71†(10.10)	**94.93**(6.17)	90.99†(10.56)
Task 4	94.14*(6.73)	**98.72**(2.34)	91.66*(9.62)
Study 2	85.63*(4.90)	**96.1**(2.68)	86.53*(4.21)

Wilcoxon rank-sum tests are performed to test if Random Forest performs statistically better than SVM and XGgoost. *: significant level at 0.05. †: significant level at 0.1.

TABLE VI
COMPARISON OF THE CLASSIFICATION USING THE PROPOSED METRICS WITH FIXED VS SUBJECT-SPECIFIC FREQUENCY BANDS FOR BRAIN OSCILLATIONS

Frequency bands	Fixed	Subject-specific
Task 1	98.95*(1.49)	**99.84**(0.65)
Task 2	99.13*(1.45)	**99.67**(1.30)
Task 3	94.47(6.81)	**94.93**(6.17)
Task 4	97.64(3.61)	**98.72**(2.34)
Study 2	95.7 (2.88)	**96.1** (2.68)

Wilcoxon rank-sum tests are performed to test if using subject-specific frequency bands shows statistically better performance than using fixed frequency bands. *: significant level at 0.05.

IV. Results and Discussion

In this section, we present the classification performance of models coupled with the proposed metrics, compare it with various features and models on Study 1 and 2, and discuss the results in terms of classification accuracy and interpretation.

A. Comparison of Scalp EEG Classification

For both study 1 and study 2, the classifiers are constructed for each subject respectively. The classification accuracy of all individuals is summarized as the mean and standard deviation in the following tables. To show the effectiveness of the classification, we compare the results in terms of classification methods, conventional versus subject-specific frequency band, and proposed metrics versus other features. Statistical analysis are also performed to test the significance of each comparison.

1) Comparison of classification methods: With the proposed metrics as features, we first test three machine learning methods and report their performance in Table V. Compared with SVM and XGboost, RF shows the highest accuracy and lowest variation across subjects. Therefore, we employ RF to build classifiers in the following comparisons.

2) Comparison of conventional frequency bands and subject-specific frequency bands: We compute the proposed metrics using two frequency bands, the conventional frequency bands and subject-specific frequency bands. The results are summarized in Table VI. Overall, using the subject-specific frequency bands can improve the classification of EEG and make the classifier more robust across individuals.

3) Comparison of the proposed metrics and other features: To test the effectiveness of the proposed metrics, we compute four sets of features that are commonly used in HHT and Wavelet transform. Three feature sets are summarized in Table VII. They are statistical features of the IMFs [6], [17], the IAs and IFs of the IMFs [18], and coefficients of wavelet [19]–[21]. To be consistent with the literature, we employ Discrete Wavelet Transform (DWT) with Daubechies4 (db4) as mother wavelet function and the number of decomposition levels to be 4. In addition, we compute another widely used feature, the power spectral density (PSD) from wavelet transform. Here, we choose the PSD of frequencies sampled in [24], where the authors sampled ~ 5 frequencies from pre-defined frequency bands for each brain oscillation. The proposed feature sets are computed using the subject-specific frequency bands.

Then, we use RF to construct the classifier for each feature sets. All classifiers are optimized and 20% of the trials are used as testing for all four tasks in study 1 and study 2. The classification performance for all subjects is summarized in Table VIII. Overall, the propose metrics with subject-specific frequency bands outperform the other four feature sets and the classifiers are more robust across individuals. The standard deviation of the accuracies at subject level are the lowest for all five cases while the mean accuracies are the highest.

The performance of DL models with HHT and wavelet as input is also reported in Table VIII. For study 1, the RF classifiers with engineered features outperform the DL models due to the unavailability of enough training data. For study 2, the DL models show comparable or even better performance compared with the RF classifiers. However, the DL model is not robust across subjects, showing the highest variation of performance for both studies.

In summary, the proposed metrics can capture the essential feature of the Hilbert spectrum, and using the subject-specific frequency bands is also helpful for addressing the inter-subject differences in the neural responses. The classifiers with the proposed metrics show the optimal classification performance and the least variation across individuals. With more trials available for training, the DL models are expected to show

TABLE VII
COMMONLY USED FEATURES IN HHT AND WAVELET

Feature set 1 [6], [17]	**Feature set 2** [18]	**Feature set 3** [19]–[21]
HHT	**HHT**	**Wavelet**
Maximum value of each IMF	Mean value of each IF	Mean absolute value of each coefficient
Minimum value of each IMF	Interquartile range (IQR) of each IF	Average power of each coefficient
Mean absolute values of each IMF	Mean absolute deviation of each IF	Standard deviation of each coefficient
Standard deviation of each IMF	Standard deviation of each IF	Mean value of each coefficient
Coefficient of variation of each IMF	Mean energy of each IA	Skewness of each coefficient
Fluctuation index of each IMF	Standard deviation of each IA	Kurtosis of each coefficient

TABLE VIII
COMPARISON OF THE CLASSIFICATION PERFORMANCE USING DIFFERENT FEATURE SETS

Methods	**Proposed Features**	**Feature Set 1**	**Feature Set 2**	**Feature Set 3**	**PSD**	**DL with HHT**	**DL with Wavelet**
Task 1	**99.84**(0.65)	99.48(1.56)	99.73(1.05)	97.63†(5.18)	97.45*(4.08)	78.57*(24.74)	80.67*(23.79)
Task 2	**99.67**(1.30)	93.27*(12.09)	95.22*(9.57)	94.81*(9.28)	95.79*(4.28)	68.56*(22.04)	64.22*(32.3)
Task 3	**94.93**(6.17)	91.78(9.08)	92.40(9.16)	93.21(8.03)	89.87*(7.80)	80.1*(21.33)	72.98*(27.17)
Task 4	**98.72**(2.34))	93.76*(7.37)	95.48*(5.33)	95.21†(6.77)	92.27*(7.84)	82.37*(18.4)	91.76*(15.71)
Study 2	**96.1**(2.68)	83.37*(4.34)	88.65*(4.28)	77.05*(3.54)	84.0*(3.69)	90.53*(8.48)	90.53*(9.11)

Wilcoxon rank-sum test are performed to test if the accuracy of the proposed method is significantly higher than the other.
*: significant level at 0.05, †: significant level at 0.1.

better performance.

B. Model Interpretation

Besides comparing the effectiveness of the proposed metrics in terms of classification, we show that the proposed metrics can also be used to indicate the connections between behavior and neural activities.

1) FR and AA can serve as informative biomarkers: The data-driven metrics FR and AA are proposed to measure the dynamic frequency components and power of brain oscillations. In addition to serving as features for building classifiers, they can be used as informative biomarkers for hypothesis testing in neuroscience research. Here, we use task 3 and 4 in study 1 as an example to illustrate how the proposed metrics support the Berger effect [36], which is a robust phenomenon in neuroscience stating that closing eyes lead to salient increases of alpha oscillations over posterior scalp EEG electrodes.

The previous scalp EEG study [24] replicated this eyes-open alpha suppression using Morlet wavelet-based power estimate procedure, which requires sampling frequencies in the predefined frequency band to represent alpha oscillation. Here, we can easily replicate the alpha power changes relevant to eyes-closure using the proposed metrics. As discussed before, the four IMFs represent distinct modes of oscillations with frequency profiles represented by FR and AA. According to FR, IMF2 is identified to serve as representative for alpha oscillation, along with the corresponding $aa_{2,2}$ measuring the power of alpha wave.

Figure 8 (a) shows the distributions of the power of alpha oscillation for CP6 electrode channel, revealing a decrease in alpha power when participant keep their eyes open. To test whether this phenomenon holds for all electrode channels, we run two sample T-test for each of the 64 channels, and report the FDR adjusted p-value in Figures 8 (b) for task 3 (moving) and 4 (standing). For both tasks, the channels in the occipital region show significant decrease in alpha power when eyes-open. Therefore, we conclude that alpha oscillations are suppressed with visual input in the occipital region, independent of movement.

2) Frontal electrodes are informative for labelling movement, and posterior electrodes for labelling on/off of visual input: The 64 electrode channels carry different amount of information with respect to the behavioral states and visual input. In study 1, we also explore the contribution of each channel in terms of differentiating behavioral states (or visual input).

For each subject, we record the top 15 features ranked by the RF classifiers according to the Gini impurity values, and mark the channels from which these features are extracted in Figure 9. The values in Figure 9 are the frequency of channels whose features are in the top ranked feature lists across all 16 individuals. Comparing the four tasks, we notice that the frontal channels carry more information in response to body movements (task 1 and 2) and the posterior electrodes are informative for labelling visual input (task 3 and 4). These qualitative findings replicate the reported results in the previous study [24] using wavelet transform. The replication suggests that the proposed metrics combined with machine learning models can capture the dynamics of neural oscillations, and have the potentials to reveal deeper links between brain and behavior.

V. FINAL REMARKS

In this paper, we have proposed a data-driven method to obtain the subject-specific frequency bands for brain oscillations, which accounts for the subject differences in neural responses. We also propose two novel metrics that compress the frequency and power information of Hilbert spectrum of the sub-signals decomposed from scalp EEG signals. The effectiveness of the proposed metrics are further tested and compared with three machine learning models and four sets of commonly used features in HHT and wavelet transform. The validation results on two scalp EEG studies show that the classifiers using the proposed metrics and the subject-specific frequency bands outperform the others and are more robust across individuals.

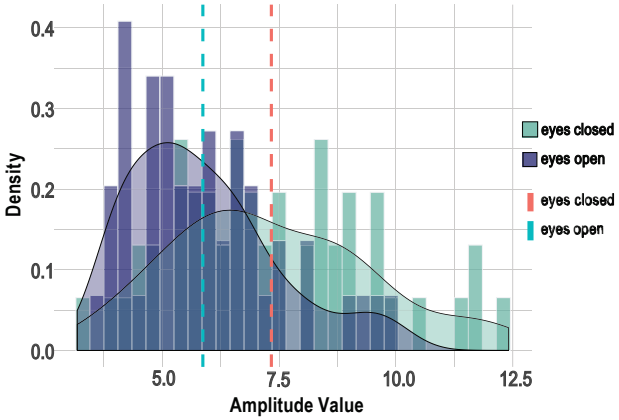

(a) Distribution of IMF 2 power

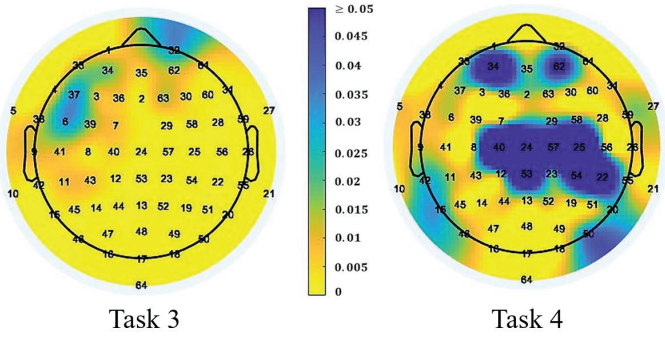

(b) P-value of the contrast (eyes open > eyes closed)

Fig. 8. (a) Distribution of the power of alpha oscillations, computed from electrode CP6 during Task 3 (Dash lines indicate group means for eyes open (green) and closed (red)); (b) shows the p-value of the hypothesis test (i.e., alpha oscillations are suppressed when eyes-open) for task 3 (switching eyes-open and eyes-closed while moving) and task 4 (switching eyes-open and eyes-closed while standing still). The color represents the FDR adjusted p-values of the electrode-wise contrasts.

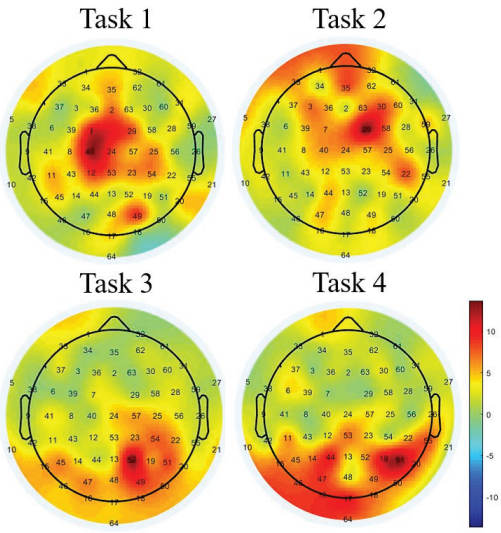

Fig. 9. Electrode channel importance in Study 1. The color represents the frequency of channels whose feature is top-ranked across all individuals. Frontal electrodes are informative for labelling movement, and posterior electrodes for labelling on/off of visual input.

In addition to classification, we demonstrate that the proposed metrics can serve as biomarkers for neuroscience research such as revealing the connections between neural oscillations and cognition. Without the need of sampling frequencies in fixed frequency bands, the proposed metrics can directly estimate the power of neural oscillations, offering an alternative for PSD. Moreover, we construct neural network architectures to automate the feature engineering process of HHT. Comparing with the ML models with engineered features, the DL models do not show advantages on both studies given that the data collected in a lab is limited. However, the DL models can achieve better performance when more data is available, such as in study 2. It is worth mentioning that the DL models are computationally expensive and give very limited interpretability.

The proposed methods can be directly applied in EEG-based brain-computer interface (BCI), which is designed to help users control external devices. The BCI identifies the user's IMAGINED body-movements by analyzing the collected scalp EEG signals and sends the command to external devices. With the proposed methods, the BCI can classify the user's imagined action more accurately and reduce the calibration time for new users, which can greatly help users with severe motor impairments.

Our empirical validation with the scalp EEG datasets opens up novel possibilities for EEG analyses. We plan to further develop effective metrics for evaluating the connectivity between electrodes, such as expanding methods developed in [37], where we propose an entropy-based metric to measure the non-linear association between EEG channels. Additionally, we are interested in discovering temporal state pattern and association network among channels for EEG signals by expanding methods developed in [38], [39]. Here, we propose that more data-driven and novel computational algorithms are needed for EEG time series analysis, and novel neural signatures linked to cognition might emerge as an outcome of data-driven algorithms and feature engineering.

Acknowledgements

The authors would like to thank the anonymous referees, an Associate Editor and the Editor for their constructive comments that improved the quality of this paper. The authors were in part supported by NSF Grant BCS-1630296.

References

[1] M. X. Cohen, "Where does eeg come from and what does it mean," *Trends in Neurosciences*, vol. 40, no. 4, pp. 208–218, 2017.

[2] W. Klimesch, "Eeg alpha and theta oscillations reflect cognitive and memory performance: a review and analysis," *Brain Research Reviews*, vol. 29, no. 2, pp. 169–195, 1999.

[3] E. Niedermeyer and F. L. da Silva, *Electroencephalography: basic principles, clinical applications, and related fields*. Lippincott Williams & Wilkins, 2005.

[4] F. L. da Silva, "Eeg and meg: relevance to neuroscience," *Neuron*, vol. 80, no. 5, pp. 1112–1128, 2013.

[5] A. D. Ekstrom and A. J. Watrous, "Multifaceted roles for low-frequency oscillations in bottom-up and top-down processing during navigation and memory." *NeuroImage*, vol. 85, pp. 667–677, 2014.

[6] R. Djemili, H. Bourouba, and M. A. Korba, "Application of empirical mode decomposition and artificial neural network for the classification of normal and epileptic eeg signals," *Biocybernetics and Biomedical Engineering*, vol. 36, no. 1, pp. 285–291, 2016.

[7] J. Skorucak, A. Hertig-Godeschalk, D. R. Schreier, A. Malafeev, J. Mathis, and P. Achermann, "Automatic detection of microsleep episodes with feature-based machine learning," *Sleep*, vol. 43, no. 1, 2020.

[8] W.-L. Zheng and B.-L. Lu, "Investigating critical frequency bands and channels for eeg-based emotion recognition with deep neural networks," *IEEE Transactions on Autonomous Mental Development*, vol. 7, no. 3, pp. 162–175, 2015.

[9] J. Jacobs, "Hippocampal theta oscillations are slower in humans than in rodents: implications for models of spatial navigation and memory," *Philosophical Transactions of the Royal Society B*, vol. 369, no. 1635, pp. 20 130 304–20 130 304, 2014.

[10] A. J. Watrous, J. Miller, S. E. Qasim, I. Fried, and J. Jacobs, "Phase-tuned neuronal firing encodes human contextual representations for navigational goals," *eLife*, vol. 7, pp. 1–16, 2018.

[11] A. J. Watrous, D. J. Lee, A. Izadi, G. G. Gurkoff, K. Shahlaie, and A. D. Ekstrom, "A comparative study of human and rat hippocampal low-frequency oscillations during spatial navigation." *Hippocampus*, vol. 23, no. 8, pp. 656–661, 2013.

[12] T. A. Whitten, A. M. Hughes, C. T. Dickson, and J. B. Caplan, "A better oscillation detection method robustly extracts eeg rhythms across brain state changes: the human alpha rhythm as a test case." *NeuroImage*, vol. 54, no. 2, pp. 860–874, 2011.

[13] A. M. Hughes, T. A. Whitten, J. B. Caplan, and C. T. Dickson, "Bosc: A better oscillation detection method, extracts both sustained and transient rhythms from rat hippocampal recordings," *Hippocampus*, vol. 22, no. 6, pp. 1417–1428, 2012.

[14] M. Doppelmayr, W. Klimesch, T. Pachinger, and B. Ripper, "Individual differences in brain dynamics: important implications for the calculation of event-related band power." *Biological Cybernetics*, vol. 79, no. 1, pp. 49–57, 1998.

[15] A. Hashemi, L. J. Pino, G. Moffat, K. J. Mathewson, C. Aimone, P. J. Bennett, L. A. Schmidt, and A. B. Sekuler, "Characterizing population eeg dynamics throughout adulthood," *ENeuro*, vol. 3, no. 6, 2016.

[16] A. J. Furman, T. J. Meeker, J. C. Rietschel, S. Yoo, J. Muthulingam, M. Prokhorenko, M. L. Keaser, R. N. Goodman, A. Mazaheri, and D. A. Seminowicz, "Cerebral peak alpha frequency predicts individual differences in pain sensitivity," *NeuroImage*, vol. 167, pp. 203–210, 2018.

[17] S. Li, W. Zhou, Q. Yuan, S. Geng, and D. Cai, "Feature extraction and recognition of ictal eeg using emd and svm," *Computers in Biology and Medicine*, vol. 43, no. 7, pp. 807–816, 2013.

[18] K. Biju, H. A. Hakkim, and M. Jibukumar, "Ictal eeg classification based on amplitude and frequency contours of imfs," *Biocybernetics and Biomedical Engineering*, vol. 37, no. 1, pp. 172–183, 2017.

[19] A. Al-Qerem, F. F. Kharbat, S. Nashwan, S. Ashraf, and khairi blaou, "General model for best feature extraction of eeg using discrete wavelet transform wavelet family and differential evolution," *International Journal of Distributed Sensor Networks*, vol. 16, no. 3, 2020.

[20] H. Hindarto, A. Muntasa, and S. Sumarno, "Feature extraction electroencephalogram (eeg) using wavelet transform for cursor movement," *IOP Conference Series: Materials Science and Engineering*, vol. 434, no. 1, p. 12261, 2018.

[21] E. Alickovic, J. Kevric, and A. Subasi, "Performance evaluation of empirical mode decomposition, discrete wavelet transform, and wavelet packed decomposition for automated epileptic seizure detection and prediction," *Biomedical Signal Processing and Control*, vol. 39, pp. 94–102, 2018.

[22] S. Patidar and T. Panigrahi, "Detection of epileptic seizure using kraskov entropy applied on tunable-q wavelet transform of eeg signals," *Biomedical Signal Processing and Control*, vol. 34, pp. 74–80, 2017.

[23] A. Delorme and S. Makeig, "Eeglab: an open source toolbox for analysis of single-trial eeg dynamics including independent component analysis," *Journal of neuroscience methods*, vol. 134, no. 1, pp. 9–21, 2004.

[24] M. Liang, M. J. Starrett, and A. D. Ekstrom, "Dissociation of frontal-midline delta-theta and posterior alpha oscillations: A mobile eeg study," *Psychophysiology*, vol. 55, no. 9, p. e13090, 2018.

[25] L. Pion-Tonachini, K. Kreutz-Delgado, and S. Makeig, "Iclabel: An automated electroencephalographic independent component classifier, dataset, and website," *NeuroImage*, vol. 198, p. 181–197, Sep 2019.

[26] M. Liang, J. Zheng, E. Isham, and A. Ekstrom, "Common and distinct roles of frontal midline theta and occipital alpha oscillations in coding temporal intervals and spatial distances," *bioRxiv*, p. 2020.08.05.237677, Jun 2021.

[27] N. E. Huang, Z. Shen, S. R. Long, M. C. Wu, H. H. Shih, Q. Zheng, N.-C. Yen, C. C. Tung, and H. H. Liu, "The empirical mode decomposition and the hilbert spectrum for nonlinear and non-stationary time series analysis," *Proceedings of the Royal Society of London. Series A: mathematical, physical and engineering sciences*, vol. 454, no. 1971, pp. 903–995, 1998.

[28] R. T. Schirrmeister, J. T. Springenberg, L. D. J. Fiederer, M. Glasstetter, K. Eggensperger, M. Tangermann, F. Hutter, W. Burgard, and T. Ball, "Deep learning with convolutional neural networks for eeg decoding and visualization." *Human Brain Mapping*, vol. 38, no. 11, pp. 5391–5420, 2017.

[29] S. Stober, A. Sternin, A. M. Owen, and J. A. Grahn, "Deep feature learning for eeg recordings," *arXiv preprint arXiv:1511.04306*, 2015.

[30] Y. R. Tabar and U. Halici, "A novel deep learning approach for classification of eeg motor imagery signals," *Journal of Neural Engineering*, vol. 14, no. 1, p. 16003, 2017.

[31] B. Xu, L. Zhang, A. Song, C. Wu, W. Li, D. Zhang, G. Xu, H. Li, and H. Zeng, "Wavelet transform time-frequency image and convolutional network-based motor imagery eeg classification," *IEEE Access*, vol. 7, pp. 6084–6093, 2019.

[32] H. Dose, J. S. Møller, H. K. Iversen, and S. Puthusserypady, "An end-to-end deep learning approach to mi-eeg signal classification for bcis," *Expert Systems with Applications*, vol. 114, pp. 532–542, 2018. [Online]. Available: https://www.sciencedirect.com/science/article/pii/S0957417418305359

[33] G. Vrbancic and V. Podgorelec, "Automatic classification of motor impairment neural disorders from eeg signals using deep convolutional neural networks," *Elektronika Ir Elektrotechnika*, vol. 24, no. 4, pp. 3–7, 2018.

[34] U. R. Acharya, S. L. Oh, Y. Hagiwara, J. H. Tan, and H. Adeli, "Deep convolutional neural network for the automated detection and diagnosis of seizure using eeg signals," *Computers in Biology and Medicine*, vol. 100, pp. 270–278, 2018. [Online]. Available: https://www.sciencedirect.com/science/article/pii/S0010482517303153

[35] D. P. Kingma and J. L. Ba, "Adam: A method for stochastic optimization," in *ICLR 2015 : International Conference on Learning Representations 2015*, 2015.

[36] H. Berger, "Über das elektrenkephalogramm des menschen," *Deutsche Medizinische Wochenschrift*, vol. 60, no. 51, pp. 1947–1949, 1934.

[37] J. Zheng, M. Liang, A. Ekstrom, L. Ge, W. Yu, and F. Hsieh, "On association study of scalp eeg data channels under different circumstances," in *International Conference on Wireless Algorithms, Systems, and Applications*. Springer, 2018, pp. 683–695.

[38] J. Zheng, H. Fushing, and L. Ge, "A data-driven approach to predict and classify epileptic seizures from brain-wide calcium imaging video data," *IEEE/ACM Transactions on Computational Biology and Bioinformatics*, pp. 1–1, 2019.

[39] F. Hsieh and J. Zheng, "Unraveling pattern-based mechanics defining self-organized recurrent behaviors in a complex system: A zebrafish's calcium brain-wide imaging example," *Frontiers in Applied Mathematics and Statistics*, vol. 5, p. 13, 2019.